NANO · MICRO small
www.small-journal.com

Smart Microcapsules with Molecular Polarity- and Temperature-Dependent Permeability

*Ji-Won Kim, Sang Seok Lee, Jinho Park, Minhee Ku, Jaemoon Yang, and Shin-Hyun Kim**

Microcapsules with molecule-selective permeation are appealing as microreactors, capsule-type sensors, drug and cell carriers, and artificial cells. To accomplish molecular size- and charge-selective permeation, regular size of pores and surface charges have been formed in the membranes. However, it remains an important challenge to provide advanced regulation of transmembrane transport. Here, smart microcapsules are designed that provide molecular polarity- and temperature-dependent permeability. With capillary microfluidic devices, water-in-oil-in-water (W/O/W) double-emulsion drops are prepared, which serve as templates to produce microcapsules. The oil shell is composed of two monomers and dodecanol, which turns to a polymeric framework whose continuous voids are filled with dodecanol upon photopolymerization. One of the monomers provides mechanical stability of the framework, whereas the other serves as a compatibilizer between growing polymer and dodecanol, preventing macrophase separation. Above melting point of dodecanol, molecules that are soluble in the molten dodecanol are selectively allowed to diffuse across the shell, where the rate of transmembrane transport is strongly influenced by partition coefficient. The rate is drastically lowered for temperatures below the melting point. This molecular polarity- and temperature-dependent permeability renders the microcapsules potentially useful as drug carriers for triggered release and contamination-free microreactors and microsensors.

Cell membrane consists of a phospholipid bilayer at which various membrane proteins are embedded. The cell membrane protects organelles in the cytoplasm from the extracellular space, while regulating transmembrane transport of various substances to interact with neighboring cells. In particular, transmembrane proteins, such as ion channels and transporters, can selectively pump specific polar ions or molecules even opposed to the natural diffusion caused by the concentration gradient.[1–3] The molecule-specific permeation through the cell membranes is of great importance in intercellular communications as well as metabolism for a living.

There have been intensive studies on artificially designing membranes with molecule-selective permeability, inspired by the cell membranes, as remarkable benefits are expected.[4,5] For example, cells can be isolated from the immune system using semipermeable capsules with a controlled cut-off threshold of permeation while secreting valuable proteins; this is referred to as immunoisolation.[6–10] The molecule-selective permeability is also useful for designing capsule-based sensors because sensing materials can be protected from contaminants to maintain high sensitivity while allowing the infusion of target molecules.[11–15] In a similar manner, enzymes or catalysts can be encapsulated to prevent contamination while allowing the exchange of reactants and products along the membrane.[16–18]

The simplest way to regulate transmembrane transport is the molecular size-selective permeation using membranes with a consistent size of pores.[19–24] To create microcapsules with regular pores in the membranes, various approaches have been employed. For example, metal–organic framework[16,17,22,25] or nanoparticles[26,27] are formed on the surface of emulsion drops through interfacial condensation or adsorption, and also a polymeric layer is prepared by a layer-by-layer (LBL) deposition.[28–31] In particular, the microcapsules prepared by LBL technology can be further designed to show pH, ionic strength, ultraviolet (UV), or temperature responsiveness, which enables the release of small molecules under the target condition.[32–36]

Recent advances in microfluidic technology have enabled the production of the double-emulsion drop, or drops-in-drop, in a highly controlled manner.[37–40] As the double-emulsion drops have a core–shell configuration, they have served as a flexible template to design functional microcapsules. To regulate transmembrane transport, the microcapsule shells have been designed to have a regular size of pores or charge. In the early development for the microcapsules with size-selective

J.-W. Kim, Dr. S. S. Lee, Prof. S.-H. Kim
Department of Chemical and Biomolecular Engineering
Korea Advanced Institute of Science and Technology (KAIST)
Daejeon 34141, Republic of Korea
E-mail: kim.sh@kaist.ac.kr
Dr. S. S. Lee
Functional Composite Materials Research Center
Institute of Advanced Composite Materials
Korea Institute of Science and Technology
Jeollabuk-do 55324, Republic of Korea
J. Park, Dr. M. Ku, Prof. J. Yang
Department of Radiology
College of Medicine
Yonsei University
Seoul 03722, Republic of Korea
The ORCID identification number(s) for the author(s) of this article can be found under https://doi.org/10.1002/smll.201900434.

DOI: 10.1002/smll.201900434

permeability, inorganic nanoparticles are assembled by solvent evaporation from the middle layer of double-emulsion drops to form a shell.[41–44] The interstitial voids among the nanoparticles have a consistent size so that size selectivity is achieved. However, the nanoparticle assemblies are mechanically unstable, which restricts the use. To improve the stability while forming the regular pores, phase separation between two polymers and microphase separation of block copolymers have been used;[20,21,23,45] the separation is caused by either solvent evaporation or polymerization of the monomer. The selective removal of one phase after the phase separation results in the regular pores in the polymer shell and the remaining monolithic shells provide a high mechanical stability. In addition, the size of pores, or equivalently the cut-off threshold of permeation, can be controlled by adjusting the degree of phase separation. The charge-selective microcapsules have been also designed by making the shell with charged hydrogel or polyelectrolyte.[46,47] However, the regulation of transmembrane transport is limited to the size and charge selection and no advanced regulation has been achieved with nonbiological materials.

Herein, we design microcapsules with a molecular polarity-dependent permeability to provide advanced transmembrane transport. With a capillary microfluidic device, water/oil/water (W/O/W) double-emulsion drops are prepared to have an oil shell containing photocurable monomers and phase-change material (PCM). The drops are irradiated with UV during the flow, which causes the polymerization of the monomers in the oil shell. The resulting membrane is composed of a cross-linked polymer framework whose voids are filled with the liquid PCM. As the PCM provides a continuous pathway, the membrane selectively allows the diffusion of molecules that are soluble in the liquid PCM. The rate of the transmembrane transport increases along with the partition coefficient of molecules in oil relative to water which depends on the polarity of molecules. The transmembrane transport can be further regulated by temperature. When the temperature is lower than the melting point of PCM, the PCM is frozen, drastically lowering solubility for all molecules. Therefore, the transport can be switched on and off depending on the temperature. These smart microcapsules that possess molecular polarity- and temperature-dependent permeability are promising for various applications including capsule-type microsensors and encapsulation of catalysts. In particular, the temperature-dependent permeability is highly beneficial for sustained release of drugs triggered by body temperature.

The smart microcapsules are designed by using W/O/W double-emulsion drops as a template, as shown in **Figure 1**a. The oil shell of double-emulsion drops is a ternary mixture of two different monomers and a liquid PCM, which turns to a solid shell through photopolymerization of the monomers. The inert PCM remains as a liquid without reaction and forms nanochannels across the entire thickness of the solid shell, serving as diffusion paths between the interior and surrounding. The rate of transmembrane transport through the PCM channels strongly depends on the solubility of molecules in the liquid PCM, thereby providing polarity-dependent permeability. At the temperatures below the melting point of the PCM, PCM is frozen so that the molecular permeability is dramatically lowered, enabling the control of permeability with external temperature.

To produce monodisperse microcapsules with a thin shell membrane, the double-emulsion drops with a thin oil layer are prepared with a glass capillary microfluidic device, as shown in Figure S1 (Supporting Information). The device consists of two tapered cylindrical glass capillaries that are coaxially aligned to have a tip-to-tip configuration inside of a square-shaped capillary.[48,49] One of the cylindrical capillaries is treated to have hydrophobic surfaces, whereas the other is to have hydrophilic surfaces. Through the hydrophobic capillary, the innermost water phase of 10 w/w% poly(vinyl alcohol) (PVA) solution and the middle oil phase of a ternary mixture of dodecanol, lauryl acrylate (LA), and trimethylolpropane ethoxylate triacrylate (ETPTA) containing 1 w/w% photoinitiator are simultaneously injected. The continuous phase has the same composition to the innermost phase, which is injected through the interstices between the hydrophobic capillary and square capillary; the interstices between the hydrophilic capillary and square capillary are sealed. The typical flow rates of the innermost, middle, and continuous phases are set to 800, 1100, and 3000 μL h^{-1}, respectively, where the device is operated at ≈45 °C to prevent freezing of dodecanol; dodecanol has a melting point of about 22–26 °C.

In the hydrophobic capillary, the water phase forms a series of plug-shaped drops without contacting the hydrophobic wall, whereas the oil phase wets the wall. This discontinuous core–sheath stream is emulsified into the continuous phase at the junction of two tapered capillaries, forming W/O/W double-emulsion drops with thin oil shell, as shown in Figure S1 and Movie S1 (Supporting Information). Due to the discontinuity of the core–sheath stream, single oil drops are also generated; the oil drops can be easily separated from the double-emulsion drops by utilizing the density difference.[49] The double-emulsion drops flow through the hydrophilic capillary and finally collected in a glass vial. To polymerize LA and ETPTA, the double-emulsion drops are irradiated by UV light during the collection. This in situ photopolymerization enables the formation of microcapsules while securing the suspension stability; bulk UV exposure after the collection frequently results in the microcapsules stuck with each other, as shown in the Figure S2 of the Supporting Information. In addition, the in situ polymerization is beneficial to make a relatively homogeneous thickness of the shell. If the drops are at rest, the density difference between the inner water droplet and the middle oil layer causes the migration of the inner droplet within the oil layer, resulting in the inhomogeneous shell after the bulk polymerization.[50] The resulting microcapsules are highly monodisperse, as shown in Figure S3 (Supporting Information); the microcapsules have an average diameter of 207 μm and its coefficient of variation of 1.39%.

The composition of the middle oil phase is set to either 29 w/w% dodecanol, 45 w/w% LA, and 25 w/w% ETPTA or 29 w/w% dodecanol, 35 w/w% LA, and 35 w/w% ETPTA to make a homogenous shell without macrophase separation based on the ternary phase diagram, as shown in Figure 1b and Figure S4 (Supporting Information). The ternary phase diagram is obtained from a set of bulk film formation tests, where the resulting films are classified to transparent, opaque, and not solidified. In common, polymerization of monomers reduces miscibility to inert liquid and causes macrophase

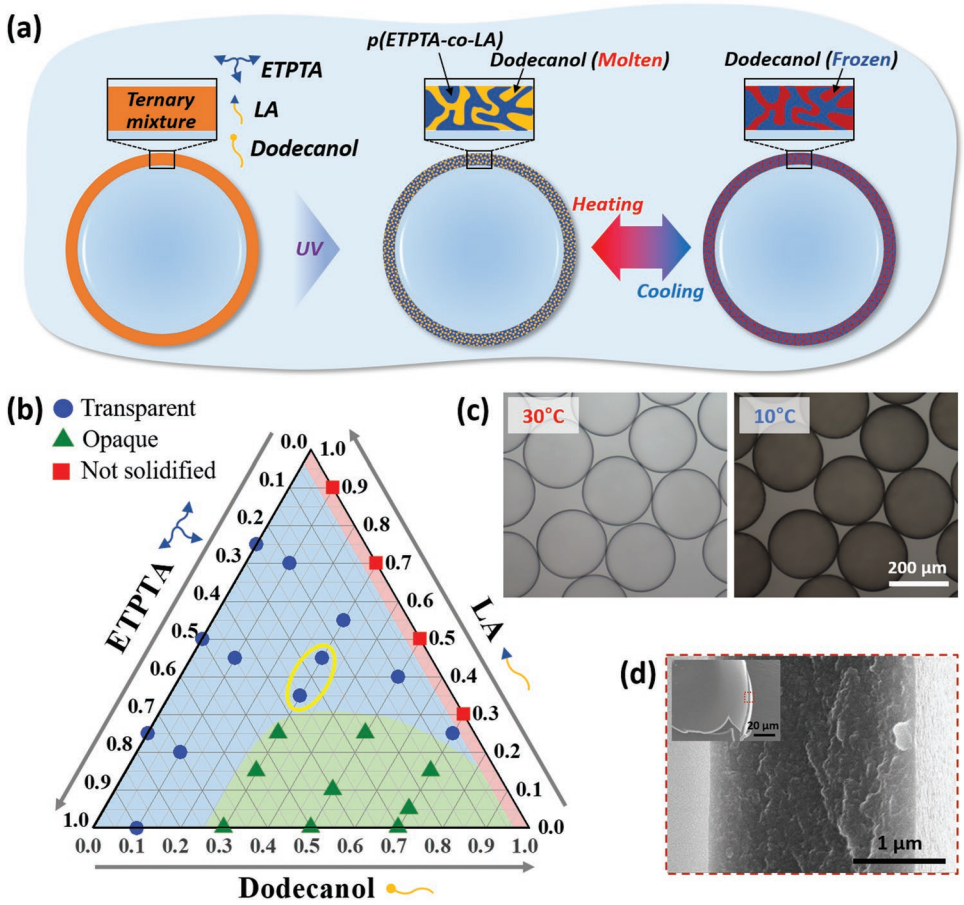

Figure 1. a) Schematic illustration for the formation of microcapsules from the double-emulsion drop by UV-induced photopolymerization of lauryl acrylate (LA) and ethoxylated trimethylolpropane triacrylate (ETPTA) in the shell of the ternary mixture and the reversible phase change of dodecanol in the void of the poly(LA-co-ETPTA) framework by heating and cooling. b) Ternary phase diagram for states of UV-irradiated mixture of ETPTA, LA, and dodecanol, where the states are classified to transparent (circles), opaque (triangles), and not solidified (squares). Two different compositions used for microcapsule production are denoted by a yellow ellipse. c) Optical microscopy (OM) images of microcapsules at two different temperatures of 30 and 10 °C, as denoted in the panels. d) Cross-sectional SEM image of the shell membrane. The inset shows a fractured microcapsule.

separation; this is known as polymerization-induced phase separation (PIPS).[21,23,51–54] The PIPS occurs when the content of LA is relatively small, producing opaque films. By contrast, a large content of LA in the mixture prevents the PIPS and produces a transparent film, as LA is highly miscible with both dodecanol and ETPTA. Therefore, LA and ETPTA form a polymeric framework through copolymerization, whereas a liquid dodecanol homogeneously fills the interstitial voids of the framework without macrophase separation. Within the domain of transparent film, the compositions are chosen to have moderate amounts of dodecanol and ETPTA to secure both the formation of continuous PCM nanochannels and high mechanical stability.

The microcapsules made from the optimized composition of oil shell are highly transparent above the melting point of dodecanol, as shown in the left panel of Figure 1c. When the temperature is lowered below the melting point, the dodecanol is frozen, rending the microcapsules translucent, as shown in the right panel. This change of transparency is reversible, as shown in Movie S2 (Supporting Information). To further confirm the absence of macrophase separation, the microcapsules are washed with isopropanol several times to remove dodecanol and observed with a scanning electron microscope (SEM), as shown in Figure 1d. The surface and cross-section of the membrane show no macropores; the membrane is ≈2.3 μm thick. By contrast, the microcapsules made from the composition forming the opaque film are not spherical and dodecanol escapes from the solid shell during the temperature swing, as shown in Figure S5 (Supporting Information). We attribute the shape deformation to the volume expansion that is concomitant with phase separation.

The membrane is composed of poly(ETPTA-co-LA) framework whose voids are filled with dodecanol. Therefore, the microcapsules are highly stable against the external shear flow and temperature change as the framework serves as solid support. This high stability is difficult to achieve with a pure dodecanol shell, as the microcapsules rupture when the dodecanol melts.[55,56] Furthermore, pure PCM shell forms cracks during freezing, which leads to leakage of encapsulants.[57,58] The dodecanol remains in the framework even for many cycles of temperature swing and does not produce cracks during freezing.

To investigate the mechanical stability, we prepare a microcapsule with a diameter of 290 µm and squeeze them with a pair of glass plates. The microcapsules are deformed to a disk shape for the compression while maintaining the shell integrity, as shown in Figure S6a (Supporting Information). The shells abruptly rupture when the strain exceeds the threshold value of 0.60. To quantitatively analyze the deformation, we measure the force during the compression using a setup composed of a syringe pump and a precision balance, as shown in Figure S6b (Supporting Information).[59] The force at fracture is estimated as 0.642 N. The stress is estimated by dividing the force with the projection area of the spherical microcapsule, from which a modulus is calculated as 15 MPa from the slope in the strain–stress curve, as shown in Figure S6c (Supporting Information).

As the dodecanol fully occupies whole voids in the framework, there is no diffusion of molecules through physical voids. However, molecules with a relatively low polarity originally dissolved in water can be transferred in the dodecanol, which then diffuses toward the other side of the membrane and finally transferred into the other water phase, as illustrated in **Figure 2**a. Rhodamine 110 chloride (R110) dissolved in the continuous phase diffuses across the membrane, gradually increasing the fluorescence intensity in the core of microcapsules, as shown in Figure 2b. The intensity saturates in

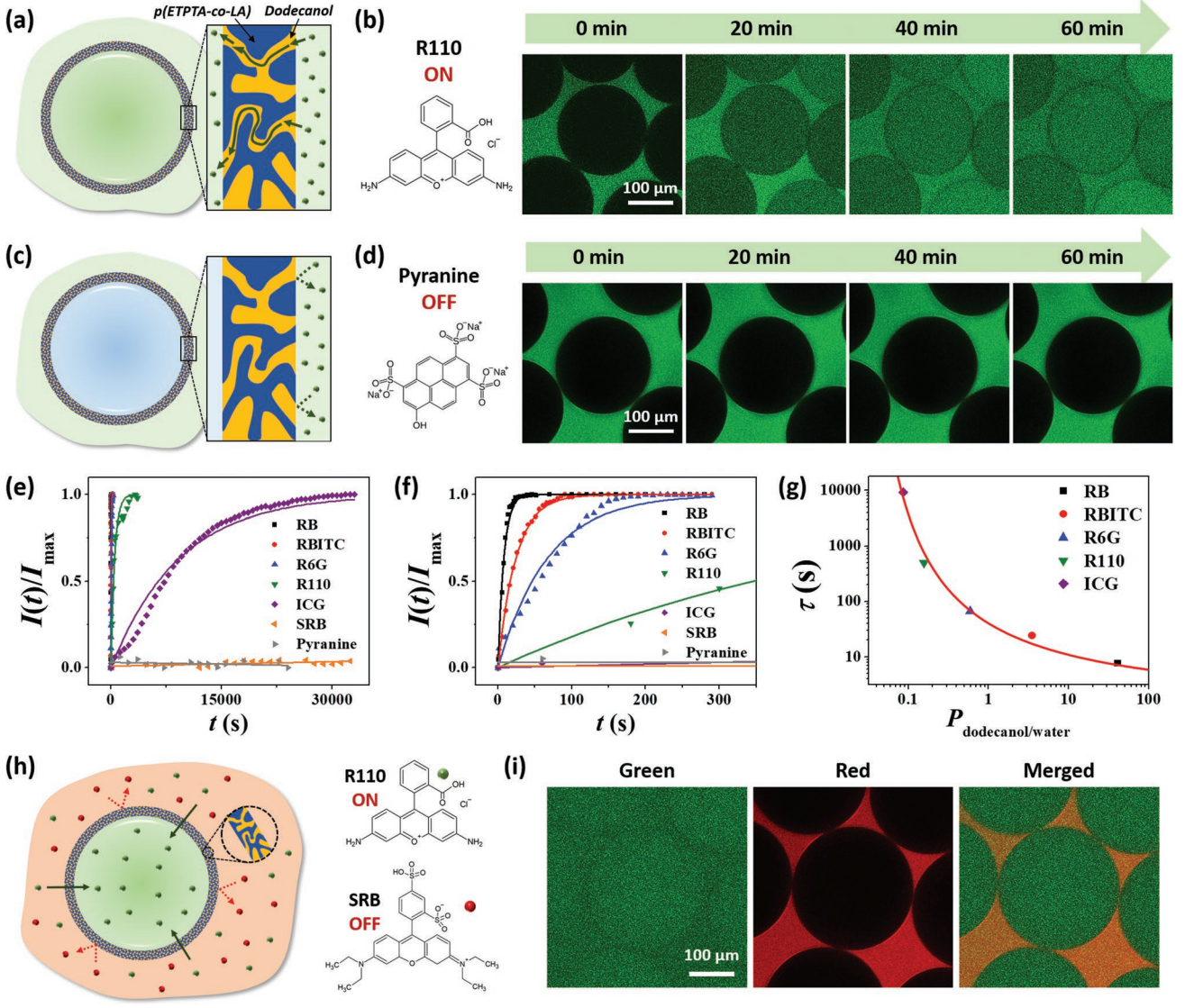

Figure 2. a) Schematic of microcapsule whose shell allows the infusion of molecules through the dissolution at the outer interface, diffusion through dodecanol nanochannel, and dissolution at inner interface. b) The molecular structure of rhodamine 110 chloride (R110) and series of confocal microscopy images showing the infusion of R110 into the core of microcapsules. c) Schematic of microcapsule whose shell rejects the molecules insoluble in dodecanol. d) The molecular structure of pyranine and series of confocal microscopy images showing the rejection of pyranine from the microcapsules. e,f) Temporal changes of normalized fluorescent intensity, $I(t)/I_{max}$, in the microcapsules for seven different dye molecules as denoted, where solid lines fit with Equation (1). g) The characteristic time scale, τ, for transmembrane permeation as a function of partition coefficient, $P_{dodecanol/water}$, for five different dyes, where solid line fits with Equation (3). h,i) Schematic and confocal microscope images of microcapsules suspended in the aqueous solution of R110 (green fluorescence) and SRB (red fluorescence), where R110 is selectively allowed to infuse into microcapsules.

1 h to be comparable to that of the surrounding. That is, the dodecanol-filled voids in the framework are interconnected to serve as diffusion paths for transmembrane transport. By contrast, molecules with high polarity are insoluble in dodecanol, which are rejected from the membrane, as illustrated in Figure 2c. For example, pyranine is not allowed to diffuse across the membrane so that fluorescence is observed from the surrounding only, as shown in Figure 2d. This set of experiments indicate that the dodecanol-polymer membranes provide molecular polarity-dependent transport; molecular weights and hydrodynamic diameters of R110 and pyranine are comparable.

To further study the influence of molecular solubility in dodecanol to the rate of the transmembrane transport, seven water-soluble dye molecules are separately dissolved in the surrounding and temporal changes in fluorescence intensity are measured at about 30 °C, as shown in Figure 2e,f. Dye molecules of rhodamine B (RB), rhodamine B isothiocyanate (RBITC), rhodamine 6G (R6G), R110, and indocyanine green (ICG) show a rapid increase at early stage and gradual saturation of the fluorescence intensity, whereas sulforhodamine B (SRB) and pyranine show no meaningful fluorescence in the timescale of 30 000 s (≈8.3 h). As the fluorescence intensity is proportional to the concentration of dye molecules, the temporal change of fluorescence can be interpreted as that of concentration. The temporal changes roughly follow the exponential function

$$\frac{I(t)}{I_{\max}} = 1 - e^{-\frac{t}{\tau}} \tag{1}$$

where $I(t)$ is time-dependent fluorescence intensity, $I_{\max}$ is the maximum intensity, and τ is the characteristic timescale for the permeation. The values of τ are 7.63, 24.1, and 66.7 s for RB, RBITC, and R6G, respectively. Therefore, it takes less than 100 s for the core of microcapsule to have a comparable concentration to the surrounding. The value of τ increases to 499 s for R110 even though free diffusion constant is almost same as RB, RBITC, and R6G. This indicates that the rate of transmembrane transport is not determined by diffusion through the PCM channels but the transfer at two interfaces of the membrane. The value of τ is as large as 9260 s for ICG and infinity for SRB and pyranine.

It is expected that the dissolution at the interface between the surrounding and membrane determines the overall dynamics of transmembrane transport. Therefore, we measure the partition coefficients of the molecules to find a relation with the rate of transport. The partition coefficient is defined as the concentration ratio in two immiscible phases of dodecanol and water at equilibrium

$$P_{\mathrm{d/w}} = \frac{c_{\mathrm{dodecanol}}}{c_{\mathrm{water}}} \tag{2}$$

To measure the values of $P_{\mathrm{d/w}}$, pure dodecanol and aqueous solution of dye molecules are incubated in a glass vial at 50 °C for a week, from which the concentrations of the dye in dodecanol and water phases are measured using absorbance spectra, as shown in Figures S7–S13 (Supporting Information); standard curves for concentration versus absorbance in dodecanol and water are obtained for all dyes to calculate the concentration in each phase from the absorbance. The characteristic timescale for transmembrane transport decreases as the partition coefficient increases as expected, as shown in Figure 2g and Table S1 (Supporting Information). We find a rough empirical relation between τ in a unit of second and $P_{\mathrm{d/w}}$ as following

$$\log \tau = \frac{1}{c_1 \log P_{\mathrm{d/w}} + c_2} \tag{3}$$

where c_1 and c_2 are found to be 0.34 and 0.62, respectively. That is, the rate of transport is very sensitive to that of dissolution, from which we conclude the overall dynamics is determined by the dissolution at the interface.

The molecular polarity-selectivity can be directly demonstrated by using a binary solution of two different dyes of one soluble in dodecanol and the other insoluble, as illustrated in Figure 2h. The microcapsules suspended in the solution of R110 and SRB show green fluorescence from the core, whereas the surrounding shows both green and red fluorescence, as shown in Figure 2i. R110 with $P_{\mathrm{d/w}}$ of 0.156 diffuses along the membrane, while SRB with $P_{\mathrm{d/w}}$ of 0.0452 is rejected. This molecule-selective permeation is very difficult to achieve with a uniform size of pores as two molecules have a comparable diameter.

The microcapsule shell provides molecular-size selectivity as well as polarity selectivity. When the microcapsules are suspended in the aqueous solution of RBITC-tagged dextran with a molecular weight of 10 000 g mol^{-1}, they do not allow the infusion of RBITC-dextran at least for 10 h, as shown in Figure S14g,h (Supporting Information). The value of $P_{\mathrm{d/w}}$ for RBITC-dextran is estimated as 0.35, from Figure S14a–f (Supporting Infromation). This value is large enough to be permeable through the shell according to Figure 2g. The rejection of RBITC-dextran is attributed to the small dimension of PCM-filled nanochannels relative to the hydrodynamic size of the molecule.

Dodecanol remains as a liquid above its melting point of 22–26 °C so that molecules can be transferred from the water. When the temperature drops below the melting point, dodecanol freezes, causing the molecules less soluble or insoluble. Therefore, transmembrane transport can be dramatically prohibited, as illustrated in **Figure 3**a. To study the temperature dependence of molecular permeation, R6G is dissolved in water at which microcapsules are subjected to three different temperatures of 30, 20, and 10 °C. In all three temperatures, the fluorescence intensity increases and gradually saturated by roughly following Equation (1). However, there is a large difference in the timescale of the transport. The fluorescence intensity in the core of microcapsule increases to be comparable to the surrounding within 80 s at 30 °C, as shown in the top row of Figure 3b and already confirmed in Figure 2e,f. The time for the intensity saturation increases to 10 min at 20 °C and 150 min at 10 °C, as shown in the middle and bottom rows of Figure 3b. The temporal changes of fluorescence intensity at 30, 20, and 10 °C are shown in Figure 3c, from which the values of τ are extracted as 66.7 s, 7.45 min, 106 min, respectively. As shown in Figure 3d, τ in a unit of second and temperature (T) in a unit of °C roughly follow an empirical relation

$$\log \tau = c_3 T + c_4 \tag{4}$$

where c_3 and c_4 are –0.099 °C^{-1} and 4.74, respectively.

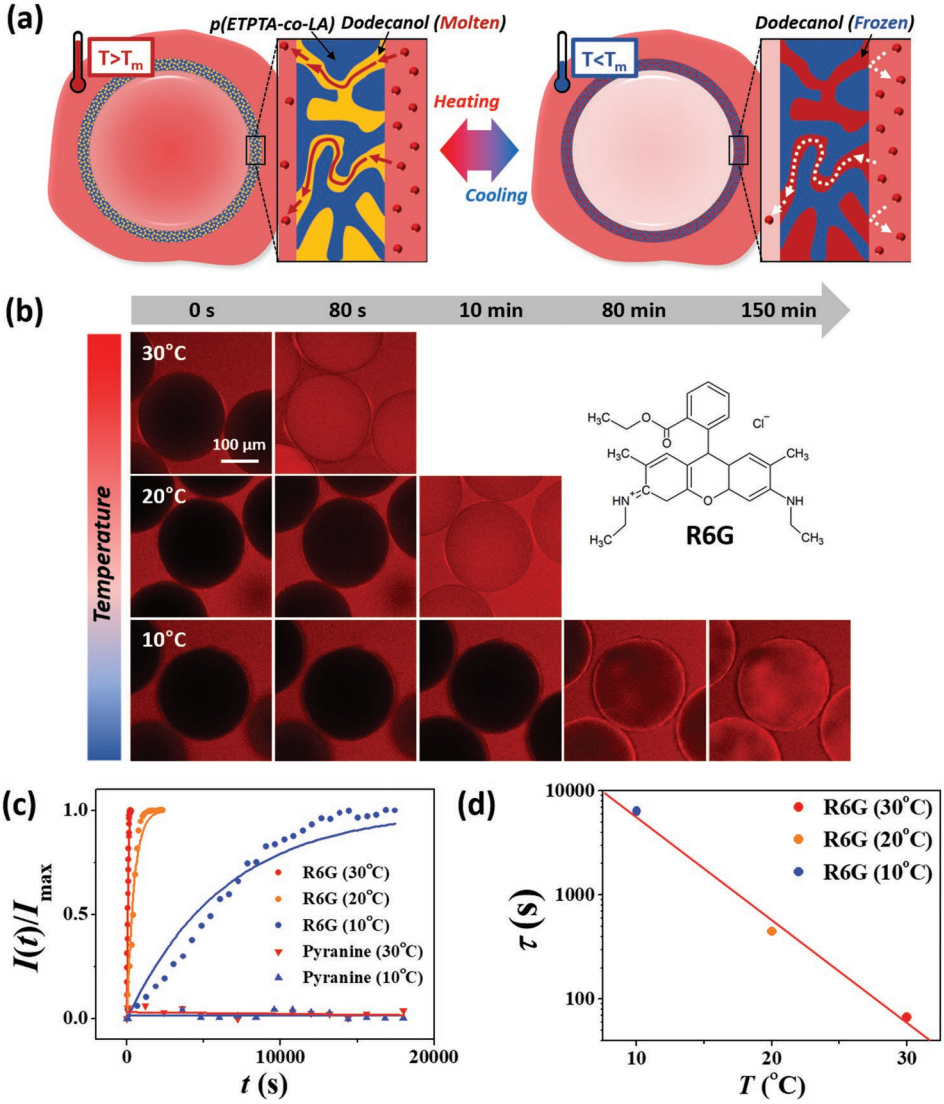

Figure 3. a) Schematics showing the reversible change between two states by heating above and cooling below the melting point of dodecanol, which are a molecule-permeable shell with molten dodecanol and molecule-impermeable or less-permeable shell with frozen dodecanol. b) Time series of confocal microscopy images showing the infusion of rhodamine 6G (R6G) at three different temperatures of 30, 20, and 10 °C, where the infusion time strongly depends on temperature. c) Temporal changes of normalized fluorescent intensity, $I(t)/I_{max}$, for R6G and pyranine at different temperatures as denoted, where solid lines fit with Equation (1). d) The characteristic time scale, τ, for transmembrane permeation as a function of temperature for R6G, where solid line fits with Equation (4).

There is a slow infusion of R6G even below the melting point of dodecanol. To confirm whether the transport is still driven by dissolution into a frozen dodecanol or by the formation of cracks, we use pyranine for a comparison. Pyranine has $P_{d/w} = 0$ at 30 °C, being rejected from the membrane. There is also no permeation at 10 °C, as shown in Figure 3c, indicating that there is no crack formation, unlike a pure PCM shell.[57,58] The dodecanol fills the molecular-scale void of the polymer framework so that freezing is unlikely to make cracks or pores. Therefore, the transmembrane transport of R6G below the melting point is purely caused by dissolution of R6G into the frozen dodecanol.

The permeation rate through the microcapsule membrane strongly depends on the molecular polarity and the temperature. Therefore, we can use the microcapsules for the temperature-triggered release of dodecanol-soluble encapsulants, as illustrated in **Figure 4**a. For a demonstrative purpose, we use ICG with $P_{d/w}$ of 0.086 as an encapsulant and analyze its release from microcapsules using absorbance of the surrounding fluid. The microcapsules show a negligible release of ICG at 4 °C for 72 h, as shown in Figure 4b. By contrast, ICG is released from the microcapsules at 37 °C. The release is relatively fast until 18 h and slows down afterward. As the rate of release depends on the temperature, the release can be switched on and off by controlling external temperature. For example, the microcapsules that retain ICG at 4 °C release ICG when the temperature is set to 37 °C for 6 h. The release is stopped when the temperature is lowered to 4 °C and the release is restarted when the temperature is raised to 37 °C, as shown in Figure 4c.

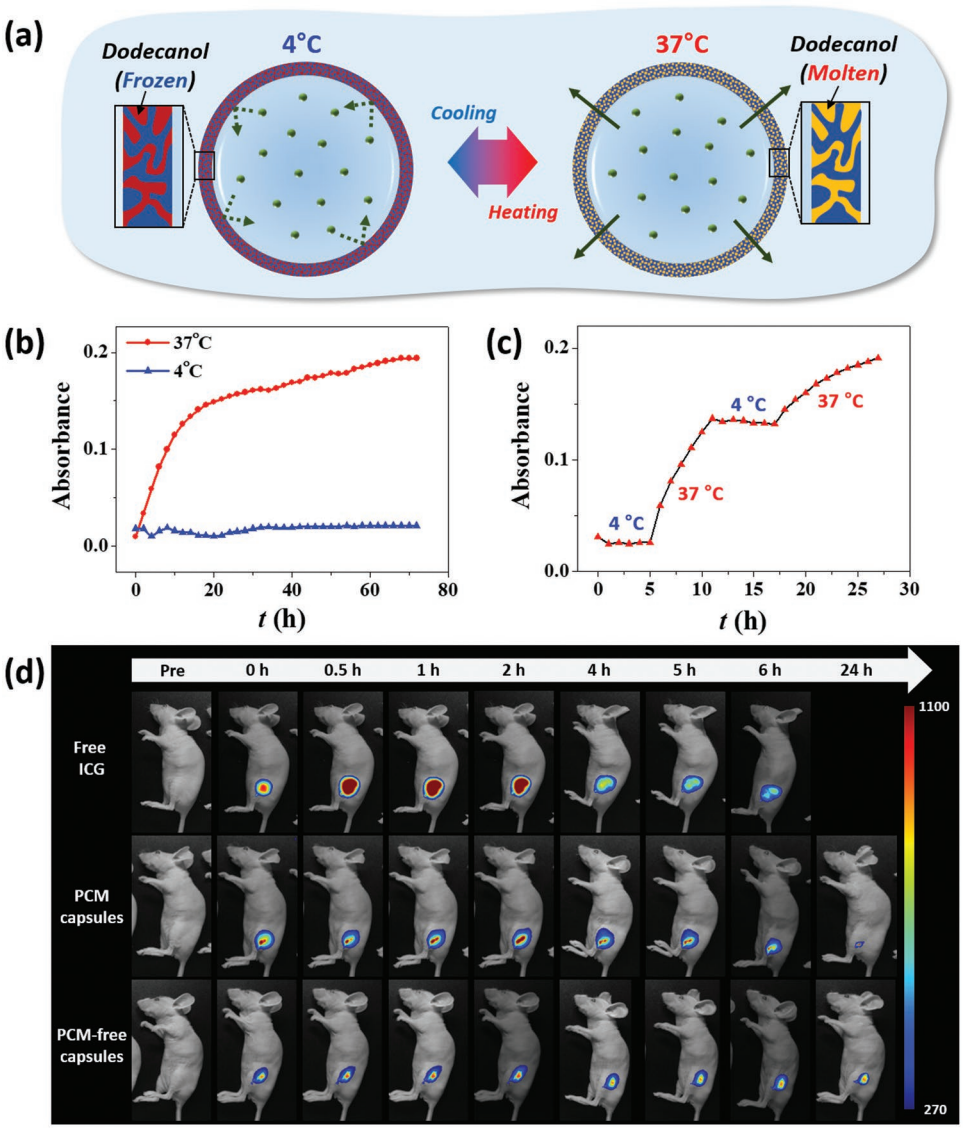

Figure 4. a) Schematic showing the preservation of encapsulants at 4 °C and the release at 37 °C. b) Temporal change of absorbance at 780 nm for the medium of indocyanine green (ICG)-loaded microcapsules at 37 and 4 °C. c) Temporal change of the absorbance for temperature change, as denoted. The microcapsules release ICG at 37 °C while retaining at 4 °C. d) Series of fluorescence images taken from mice for 24 h after injecting free ICG solution (top), ICG-loaded microcapsules (middle), and ICG-loaded PCM-free microcapsules (bottom).

The microcapsules with temperature sensitivity are useful for a localized, sustained release of drugs when implanted in tissue while preserving the drug with the refrigeration. As the microcapsules are small enough to be injected using a needle without a clogging problem and large enough to be fixed at the tissue, they can be easily implanted in the injection site. To confirm the body temperature-triggered release, the microcapsules containing ICG are implanted in the thigh of nude mice through a subcutaneous injection and fluorescent signal is monitored for 24 h; body temperature of the mouse is typically 36.5–38.0 °C.[60] For comparison, free ICG solution is injected in the same manner. The free ICG solution rapidly spreads over the body in 2 h and gradually fades out afterward, as shown in the top row of Figure 4d. The temperature-sensitive microcapsules show a different release behavior, as shown in the middle row. First of all, there is almost no time-dependent spreading as the ICG-laden microcapsules are implanted on the injection site. The fluorescent intensity gradually decreases after 2 h, as ICG is slowly yet continuously released from the microcapsules. In 24 h, the fluorescence almost dies out. The release of ICG is localized near the injection site so that the site is constantly exposed to ICG during the period of the sustained release; this contrasts to the injection of the free ICG which increases the concentration of ICG at the moment of the injection and rapidly decreases it as ICG rapidly spreads over the whole body. The timescale for the release from the microcapsules is roughly 20 h, which is comparable to that in phosphate buffered saline (PBS) solution at 37 °C. To confirm that the release is not caused by a failure of microcapsule membrane, the skin on the injection site is incised and the

microcapsules are recovered from the tissue underneath the skin after 24 h. The recovered microcapsules remain intact, as shown in Figure S15 (Supporting Information). The recovered microcapsules contain ICG at the reduced concentration from the initial state due to the release; although fluorescence intensity is very low at 24 h, it is high after the incision of the skin because the optical barrier is removed, as shown in Figure S15 (Supporting Information). To further study the temperature sensitivity, we prepare PCM-free microcapsules containing ICG, where the membrane of PCM-free microcapsules is made of polymerized ETPTA only. The PCM-free microcapsules are insensitive to temperature so that they show a consistent fluorescence over 24 h when implanted, as shown in the bottom row of Figure 4d. This is because the membrane does not allow the diffusion of ICG. This comparative experiment further confirms that PCM is prerequisite to endow the temperature-triggered release of encapsulants.

In this work, we design smart microcapsules whose shell membranes have molecular polarity- and temperature-dependent permeability. The microcapsules are microfluidically prepared from W/O/W double-emulsion template to have uniform size and composition, of which shell consists of cross-linked polymer framework whose continuous voids are filled with PCM. The shell is carefully designed by polymerizing monomers in the presence of PCM while preventing macrophase separation between the growing polymer and PCM by introducing a molecular compatibilizer. Above the melting point of PCM, the molecules that are soluble in the molten PCM are allowed to diffuse across the shell, where the rate of the transmembrane transport is strongly influenced by the partition coefficient of the molecules. By contrast, the molecules that are insoluble in the molten PCM are rejected from the microcapsules. The transport is highly suppressed even for the molecules soluble in the PCM when the temperature drops below the melting temperature as the PCM is frozen. Although various types of microcapsules with regular size of nanopores and surface charges have been reported to provide molecular size- and charge-dependent permeability, there has been no experimental demonstration and systematic study on such an advanced regulation of transmembrane transport. The polarity-dependent permeation property enables the selective infusion of less-polar molecules while rejecting more-polar molecules even if these molecules have comparable size. This molecular selection is potentially beneficial for improving the performance of microreactors and capsule-type molecular sensors by excluding more-polar contaminants. In addition, the temperature-dependent permeation enables the stable storage of encapsulants at low temperature and the controlled release of them at body temperature. Therefore, it is possible to retain drugs in the capsules while keeping in the refrigerator and release them in a localized and sustained fashion when implanted in a body, as we demonstrated; most drugs are not highly soluble in water and applicable to our microcapsules. It is expected that the release rate can be further tuned according to the selection of PCM for a target drug. As the setting temperature can be increased slightly above the body temperature by selecting a proper PCM, it is also possible to design microcapsules that release the encapsulants under external heating after being implanted. To show the possibility to use various PCM materials, we prepare microcapsules whose solid shell contains undecanol and 1-tetradecanol, as shown in Figure S16 (Supporting Information); undecanol and 1-tetradecanol have melting points of 19 and 38 °C, respectively. The microcapsules show a reversible change of transparency during temperature swing above and below the melting point and no PCM escapes from the shell, in the same manner to the microcapsules containing dodecanol. In addition, the polarity selection and temperature response are also confirmed for the microcapsules containing undecanol. We believe that this advanced transmembrane transport property of the microcapsules, combined with high controllability of microfluidic technology, will provide new opportunities in a wide range of applications as drug carriers, microreactors, and microsensors.

Experimental Section

Preparation of Capillary Microfluidic Devices: The glass capillary microfluidic device was comprised of two cylindrical capillaries (OD 1.0 mm, ID 0.58 mm, World Precision Instruments) assembled in one square-shaped capillary (OD 1.5 mm, ID 1.05 mm, Atlantic International Technologies, Inc.), as shown in Figure S1 (Supporting Information). The square-shaped glass capillary was fixed on the transparent slide glass by using epoxy glue. Two cylindrical capillaries were tapered by using micropipette puller (P-97, Sutter Instrument) and sanded by using a paper to make the tip with desired diameter: 240 µm for injection capillary and 280 µm for collection capillary. After washing with distilled water and complete drying, the capillary with 240 µm orifice was dipped in 2-[methoxy(polyethyleneoxy)propyl]trimethoxy silane (Gelest, Inc.) for 25 min to render the surface hydrophobic and the capillary with 280 µm orifice was dipped in trimethoxy(octadecyl) silane (Sigma-Aldrich) to render the surface hydrophilic. After washing them with isopropanol and distilled water each, capillaries were dried completely and coaxially aligned in the middle of the square-shaped capillary to have a tip-to-tip separation of 200 µm. After fixing the capillaries on the slide glass with epoxy glue, the additional cylindrical capillary was tapered and inserted into the untapered opening of the hydrophobic injection capillary. The openings of cylindrical and square capillaries were connected with needles and sealed by epoxy glue to inject fluids.

Preparation and Characterization of Microcapsules: For construction of ternary phase diagram, various compositions of the ternary mixtures containing 1 w/w% photoinitiator of 2-hydroxy-2-methylpropiophenone (Darocur 1173, 97%, Sigma-Aldrich) were prepared, where the three components were the dodecanol (M_w 186.33 g mol^{-1}, Sigma-Aldrich), LA (M_w 240.38 g mol^{-1}, Sigma-Aldrich), and ETPTA (M_n 428 g mol^{-1}, Sigma-Aldrich). The ternary mixtures were infiltrated into a gap between two parallel glass substrates, which were then irradiated by spot UV (Innocure, Lichtzen) for 2 min. The resulting films were classified into transparent, opaque, and not solidified, as shown in Figure S4a (Supporting Information).

To make microcapsules, an aqueous solution of 10 w/w% PVA (M_w 13 000–23 000 g mol^{-1}, Sigma-Aldrich) was used as innermost and continuous phase. The composition of the middle oil phase was set to 29 w/w% dodecanol, 45 w/w% LA, and 25 w/w% ETPTA to make homogeneous shells of microcapsules based on the ternary phase diagram. For the release study, the aqueous solution of 10 w/w% PVA and 130×10^{-3} M sucrose (M_w 342.30 g mol^{-1}, Sigma-Aldrich) containing 1.3×10^{-3} M ICG, and the aqueous solution with 10 w/w% PVA and 0.62 × PBS solution (20×, LPS solution) were used as the innermost phase and the continuous phase respectively, whereas the composition of the oil phase was set to 29 w/w% dodecanol, 35 w/w% LA, and 35 w/w% ETPTA; the osmolarities of the innermost and continuous solutions were set to 300 mOsm L^{-1} for in vivo study. The innermost, middle, and continuous phases were injected using syringe pumps (Legato 100, KD Scientific) through polyethylene tubing (OD 1.32 mm,

ID 0.86 mm, Scientific Commodities, Inc.), where the temperature was set to 45 °C. Drop generation was observed by using an inverted optical microscope (Eclipse TS100, Nikon) equipped with a high-speed camera (MotionScope M3, Redlake). The double-emulsion drops were collected in 3 w/w% PVA solution and continuously irradiated by spot UV. For the microcapsules for in vivo release study, the double-emulsion drops were collected in an aqueous solution of 3 w/w% PVA and 0.89 × PBS solution with osmolarity of 300 mOsm L^{-1} for 1 h, which were then exposed by a box UV (System Korea) for 90 s to minimize photobleaching of dye loaded in the core. Resultant microcapsules were washed with distilled water or 1 × PBS solution, depending on the osmolarity of the core, and stored at 4 °C in the refrigerator.

The microcapsules in water were observed with an optical microscope (Eclipse L150, Nikon), where a heating stage (T96, Linkam Scientific Instruments) was used to set sample temperature. The surface and cross-section of membranes were observed with a SEM (S-4800, Hitachi) after coating with osmium tetroxide, where the microcapsules were washed with isopropanol to remove dodecanol and completely dried before the sample preparation. To estimate the partition coefficient of dye molecules, UV/Visible spectrophotometer (3220UV, Optizen) was used.

Characterization of Transmembrane Transport: To study transmembrane transport, fluorescent dye molecules of SRB (M_w 580.65 g mol^{-1}, Sigma-Aldrich), R6G (M_w 479.01 g mol^{-1}, Sigma-Aldrich), RB (M_w 479.01 g mol^{-1}, Sigma-Aldrich), RBITC (M_w 536.08 g mol^{-1}, Sigma-Aldrich), R110 (M_w 366.80 g mol^{-1}, Sigma-Aldrich), 8-hydroxypyrene-1,3,6-trisulfonic acid trisodium salt (pyranine, M_w 524.39 g mol^{-1}, Sigma-Aldrich), and ICG (M_w 774.96 g mol^{-1}, Sigma-Aldrich) were used. Two opposite directions of transport, infusion into microcapsules and release from the microcapsules, were studied. For the infusion, the microcapsules were suspended in the aqueous solution of selected dye and repeatedly observed with a laser scanning confocal microscope (LSM 5 PASCAL, Carl Zeiss). For the release, the microcapsules containing 1.3 × 10^{-3} M ICG were suspended in 1 × PBS solution and the supernatant was continuously analyzed with a UV/Visible spectrophotometer (UV-1900, Shimadzu), where the temperature of the cuvette was maintained using the water circulator (AD-RC08i, BNC Korea).

In Vivo Release Study: To study the release of ICG in the in vivo environment, the microcapsules were implanted to the thigh of female nude mice (BALB/C-nude, average 17 g) through a subcutaneous injection using a 22 gauge needle (Korea Vaccine co. Ltd), from which fluorescence images were repeatedly acquired for 24 h. The mice were anesthetized with a mixture of Zoletil50 (Virbac) and Rompun (Bayer Korea) by intraperitoneal injection (30 µL, 3:1 ratio). A capsule-free aqueous solution of 0.003 × 10^{-3} M ICG and microcapsules with a shell made of polymerized ETPTA were injected by following the same protocol as controls. In vivo fluorescence imaging was conducted using the InVivo Smart fluorescent imaging and analysis system (Visque, Vieworks), where background fluorescence signals were adjusted. After 24 h, the mouse skins around the injection spot were lifted with forceps and incised, while fluorescently imaging the site. The interrogated tissues were extracted after the removal of skin, which were then immersed in 1 × PBS solution. The microcapsules recovered from the tissues were observed with an inverted optical microscope (Eclipse Ti-U, Nikon). All in vivo experiments were conducted with the approval of the Association for Assessment and Accreditation of Laboratory Animal Care (AAALAC) International.

Supporting Information

Supporting Information is available from the Wiley Online Library or from the author.

Acknowledgements

This research was supported by the National Research Foundation (NRF) (Grant Nos. NRF-2017R1A2A2A05001156, NRF-2015K1A1A2033054, and NRF-2017R1C1B2010867) funded by the Ministry of Science, ICT, and Future Planning (MSIP) and the Korea Health Industry Development Institute (KHIDI) (Grant No. HI17C2586) funded by the Ministry of Health and Welfare. J.-W.K. appreciates the Global Ph.D. Fellowship Program (Grant No. NRF-2018H1A2A1061048) of the NRF.

Conflict of Interest

The authors declare no conflict of interest.

Keywords

microcapsules, microfluidics, phase-change materials, selective permeation, transmembrane transport

Received: January 24, 2019
Revised: March 14, 2019
Published online:

[1] N. A. Bradbury, R. J. Bridges, *Am. J. Physiol.* **1994**, *267*, C1.
[2] K. Simons, E. Ikonen, *Nature* **1997**, *387*, 569.
[3] G. van Meer, D. R. Voelker, G. W. Feigenson, *Nat. Rev. Mol. Cell Biol.* **2008**, *9*, 112.
[4] M. Garni, S. Thamboo, C.-A. Schoenenberger, C. G. Palivan, *Biochim. Biophys. Acta, Biomembr.* **2017**, *1859*, 619.
[5] N. Ben-Haim, P. Broz, S. Marsch, W. Meier, P. Hunziker, *Nano Lett.* **2008**, *8*, 1368.
[6] T. M. S. Chang, *Science* **1964**, *146*, 524.
[7] T. M. S. Chang, *Nature* **1971**, *229*, 117.
[8] F. Lim, A. M. Sun, *Science* **1980**, *210*, 908.
[9] A. C. Powers, M. Brissová, I. Lacík, A. V. Anilkumar, K. Shahrokhi, T. G. Wang, *Ann. N. Y. Acad. Sci.* **2006**, *831*, 208.
[10] B. P. Barnett, A. Arepally, M. Stuber, D. R. Arifin, D. L. Kraitchman, J. W. M. Bulte, *Nat. Protoc.* **2011**, *6*, 1142.
[11] S. Chinnayelka, M. J. McShane, *Anal. Chem.* **2005**, *77*, 5501.
[12] O. Kreft, A. M. Javier, G. B. Sukhorukov, W. J. Parak, *J. Mater. Chem.* **2007**, *17*, 4471.
[13] X. Xie, W. Zhang, A. Abbaspourrad, J. Ahn, A. Bader, S. Bose, A. Vegas, J. Lin, J. Tao, T. Hang, H. Lee, N. Iverson, G. Bisker, L. Li, M. S. Strano, D. A. Weitz, D. G. Anderson, *Nano Lett.* **2017**, *17*, 2015.
[14] C. H. Park, S. Lee, G. Pornnoppadol, Y. S. Nam, S.-H. Kim, B. J. Kim, *ACS Appl. Mater. Interfaces* **2018**, *10*, 9023.
[15] S. Lee, T. Y. Lee, D. J. Kim, B. Kim, S.-H. Kim, *Chem. Mater.* **2018**, *30*, 7211.
[16] J. Huo, J. Aguilera-Sigalat, S. El-Hankari, D. Bradshaw, *Chem. Sci.* **2015**, *6*, 1938.
[17] L. Lin, T. Zhang, H. Liu, J. Qiu, X. Zhang, *Nanoscale* **2015**, *7*, 7615.
[18] L. D. Blackman, S. Varlas, M. C. Arno, Z. H. Houston, N. L. Fletcher, K. J. Thurecht, M. Hasan, M. I. Gibson, R. K. O'Reilly, *ACS Cent. Sci.* **2018**, *4*, 718.
[19] M. Ali, S. Bora, S. K. Ghosh, *Langmuir* **2014**, *30*, 10449.
[20] B. Kim, T. Y. Lee, A. Abbaspourrad, S.-H. Kim, *Chem. Mater.* **2014**, *26*, 7166.
[21] B. Kim, T. Y. Jeon, Y.-K. Oh, S.-H. Kim, *Langmuir* **2015**, *31*, 6027.
[22] W. Li, Y. Zhang, Z. Xu, Q. Meng, Z. Fan, S. Ye, G. Zhang, *Angew. Chem., Int. Ed.* **2016**, *55*, 955.
[23] J. Oh, B. Kim, S. Lee, S.-H. Kim, M. Seo, *Chem. Mater.* **2018**, *30*, 273.
[24] X. Hao, L. Chen, W. Sang, Q. Yan, *Adv. Sci.* **2018**, *5*, 1700591.

[25] C. Doonan, R. Riccò, K. Liang, D. Bradshaw, P. Falcaro, *Acc. Chem. Res.* **2017**, *50*, 1423.
[26] D. Patra, A. Sanyal, V. M. Rotello, *Chem.- Asian J.* **2010**, *5*, 2442.
[27] D. Patra, F. Sleem, *Colloids Surf., A* **2014**, *443*, 320.
[28] W.-F. Dong, J. K. Ferri, T. Adalsteinsson, M. Schönhoff, G. B. Sukhorukov, H. Möhwald, *Chem. Mater.* **2005**, *17*, 2603.
[29] E. W. Stein, D. V. Volodkin, M. J. McShane, G. B. Sukhorukov, *Biomacromolecules* **2006**, *7*, 710.
[30] P. K. Mandapalli, S. Labala, D. Vanamala, M. P. Koranglekar, L. A. Sakimalla, V. V. K. Venuganti, *Drug Delivery* **2014**, *21*, 605.
[31] A. Biswas, A. T. Nagaraja, Y.-H. You, J. R. Roberts, M. J. McShane, *RSC Adv.* **2016**, *6*, 71781.
[32] M. Prevot, C. Déjugnat, H. Möhwald, G. B. Sukhorukov, *Chem. Phys. Chem.* **2006**, *7*, 2497.
[33] V. Kozlovskaya, E. Kharlampieva, I. Drachuk, D. Cheng, V. V. Tsukruk, *Soft Matter* **2010**, *6*, 3596.
[34] Q. Yi, G. B. Sukhorukov, *ACS Nano* **2013**, *7*, 8693.
[35] W. Xu, A. A. Steinschulte, F. A. Plamper, V. F. Korolovych, V. V. Tsukruk, *Chem. Mater.* **2016**, *28*, 975.
[36] W. Xu, P. A. Ledin, Z. Iatridi, C. Tsitsilianis, V. V. Tsukruk, *Angew. Chem., Int. Ed.* **2016**, *55*, 4908.
[37] S. S. Lee, A. Abbaspourrad, S.-H. Kim, *ACS Appl. Mater. Interfaces* **2014**, *6*, 1294.
[38] T. Y. Lee, T. M. Choi, T. S. Shim, R. A. M. Frijns, S.-H. Kim, *Lab Chip* **2016**, *16*, 3415.
[39] C.-X. Zhao, D. Chen, Y. Hui, D. A. Weitz, A. P. J. Middelberg, *Chem. Phys. Chem.* **2016**, *17*, 1553.
[40] C.-X. Zhao, D. Chen, Y. Hui, D. A. Weitz, A. P. J. Middelberg, *Chem. Phys. Chem.* **2017**, *18*, 1393.
[41] D. Lee, D. A. Weitz, *Adv. Mater.* **2008**, *20*, 3498.
[42] R. K. Shah, J.-W. Kim, D. A. Weitz, *Crit. Rev. Ther. Drug Carrier Syst.* **2010**, *26*, 1561.
[43] J. S. Sander, A. R. Studart, *Langmuir* **2011**, *27*, 3301.
[44] T. Brugarolas, F. Tu, D. Lee, *Soft Matter* **2013**, *9*, 9046.
[45] R. A. Prasath, M. T. Gokmen, P. Espeel, F. E. Du Prez, *Polym. Chem.* **2010**, *1*, 685.
[46] G. Kaufman, R. Boltyanskiy, S. Nejati, A. R. Thiam, M. Loewenberg, E. R. Dufresne, C. O. Osuji, *Lab Chip* **2014**, *14*, 3494.
[47] L. Zhang, L.-H. Cai, P. S. Lienemann, T. Rossow, I. Polenz, Q. Vallmajo-Martin, M. Ehrbar, H. Na, D. J. Mooney, D. A. Weitz, *Angew. Chem.* **2016**, *128*, 13668.
[48] A. S. Utada, E. Lorenceau, D. R. Link, P. D. Kaplan, H. A. Stone, D. A. Weitz, *Science* **2005**, *308*, 537.
[49] S.-H. Kim, J. W. Kim, J.-C. Cho, D. A. Weitz, *Lab Chip* **2011**, *11*, 3162.
[50] S. S. Datta, S.-H. Kim, J. Paulose, A. Abbaspourrad, D. R. Nelson, D. A. Weitz, *Phys. Rev. Lett.* **2012**, *109*, 134302.
[51] H. M. J. Boots, J. G. Kloosterboer, C. Serbutoviez, F. J. Touwslager, *Macromolecules* **1996**, *29*, 7683.
[52] C. Serbutoviez, J. G. Kloosterboer, H. M. J. Boots, F. J. Touwslager, *Macromolecules* **1996**, *29*, 7690.
[53] J.-W. Kim, K.-S. Lee, H.-K. Ju, J.-H. Ryu, S.-H. Han, I.-S. Chang, H.-H. Kang, S.-G. Oh, K.-D. Suh, *J. Polym. Sci., Part A: Polym. Chem.* **2004**, *42*, 2202.
[54] W. Liu, Y. Zhao, C. Zeng, C. Wang, C. A. Serra, L. Zhang, *Chem. Eng. J.* **2017**, *307*, 408.
[55] B. J. Sun, H. C. Shum, C. Holtze, D. A. Weitz, *ACS Appl. Mater. Interfaces* **2010**, *2*, 3411.
[56] M. Windbergs, Y. Zhao, J. Heyman, D. A. Weitz, *J. Am. Chem. Soc.* **2013**, *135*, 7933.
[57] Y. Zhao, H. C. Shum, L. L. A. Adams, B. Sun, C. Holtze, Z. Gu, D. A. Weitz, *Langmuir* **2011**, *27*, 13988.
[58] T. A. Comunian, A. Abbaspourrad, C. S. Favaro-Trindade, D. A. Weitz, *Food Chem.* **2014**, *152*, 271.
[59] S. S. Lee, J. Park, Y. Seo, S.-H. Kim, *ACS Appl. Mater. Interfaces* **2017**, *9*, 17178.
[60] M. A. Suckow, P. Danneman, C. Brayton, *The Laboratory Mouse*, CRC Press, Boca Raton **2001**.

